Structure of the Surface of a Surfactant Solution above the Critical Micelle Concentration

J. R. Lu, E. A. Simister, and R. K. Thomas*

Physical Chemistry Laboratory, South Parks Road, Oxford, OX1 3QZ, U.K.

J. Penfold

Rutherford-Appleton Laboratory, Chilton, Didcot, Oxon, U.K.

Received: July 12, 1993; In Final Form: October 11, 1993®

The adsorption at the air/solution interface of the surfactant tetradecyltrimethylammonium bromide (C_{14}TAB) above its critical micelle concentration (cmc = 3.7 mM) has been studied by neutron specular reflection. The amount adsorbed increases with concentration steadily through and above the cmc. Combination of the surface tension and the surface excess, as determined by neutron reflection, has been used to determine the variation of the activity of the surfactant from the cmc up to 0.16 M. The structure of the adsorbed layer at a concentration 50 times the cmc is shown to consist of the usual monolayer of surfactant, an aqueous layer from which surfactant is absent, and a further layer of surfactant with about a 5% excess over the bulk solution. The width and concentration of this lower surfactant layer suggests that it corresponds to an adsorbed layer of micelles and that the center of this layer is located at approximately 90 Å from the center of the monolayer, making the aqueous layer about 55 Å thick. The net positive adsorption of micelles in the region below the monolayer indicates that there is an effective attractive interaction between micelles and the "wall", which may result from the monolayer/micelle interaction being less repulsive than the micelle/bulk solution interaction. There is some, less conclusive, indication that the aqueous layer may also be structured near the monolayer.

Introduction

Although most of the technological applications of surfactant solutions involve their use at concentrations above the critical micelle concentration (cmc), little is known about the structure of the surface of such solutions. This is in part because there has been no experimental technique which gives structural information about such surfaces and in part because it is difficult to apply the Gibbs equation to surface tension data. The second point is illustrated by the best studied system, sodium dodecyl sulfate (SDS) in water.[1,2] The gradient of a surface tension (γ)–log(activity) plot should give the surface excess directly, and although we have recently shown that great care has to be taken to obtain accurate values of the surface excess,[3] there are no fundamental obstacles below the cmc. To a good approximation, the activity may be taken to be the same as the concentration. Above the cmc there are two problems. One is the experimental problem that the change in γ with concentration is much smaller than below the cmc and therefore has to be measured with higher precision. The second and more serious problem is that the activity not only is not related simply to the concentration but also, like the surface tension, is varying very slowly, and this variation is experimentally somewhat inaccessible. However, Hall et al.[2] have used this method to deduce that the surface excess of SDS increases above the cmc. The only direct measurements of surface excess above the cmc are radiotracer measurements, e.g. ref 4, and these suffer from the uncertain assumptions that have to be made about scaling and background subtraction.

A knowledge of the surface excess gives no information about the structure of the interface, and structural information is necessary if any successful modeling of such interfaces is to be made. We have shown that neutron reflection is a powerful technique for determining the structures of the surfaces of surfactant solutions below the cmc,[5] and here we extend it to a system above the cmc. We have already published preliminary data on neutron reflection from solutions of protonated surfactant in D_2O, which indicated that the structure of the surface is more complex than just a single monolayer of surfactant.[6,7] However, those data were incomplete because an accurate assessment of the background scattering could not be made at the time, and it was not possible to make the complementary measurements on the fully deuterated surfactants, which are necessary to elucidate the structure. However, the main conclusion that there is longer-range ordering at the interface has been substantiated by computer simulation.[8,9] Here we present a more complete study of tetradecyltrimethylammonium bromide (C_{14}TAB) above the cmc.

Experimental Details

Two isotopic species of tetradecyltrimethylammonium bromide were used in the experiments, $C_{14}D_{29}N(CD_3)_3Br$ and $C_{14}H_{29}N(CH_3)_3Br$, which we refer to as dC_{14}dTAB and hC_{14}hTAB, respectively. The method of preparation and purification has been described by Simister et al.[3,5] The raw materials used for the preparations were $C_{14}D_{29}Br$ and $N(CD_3)_3$ from Merck, Sharp & Dohme. At least two and sometimes as many as five recrystallizations of the crude surfactant were usually necessary to obtain satisfactory purity as assessed from surface tension measurements. High-purity water was used throughout (Elga Ultrapure system), and the methods of cleaning the glassware and Teflon troughs for the neutron experiment were as described in ref 3. The experiments were performed at 298 K.

The neutron reflection measurements were made on the reflectometer CRISP at the Rutherford-Appleton Laboratory (Didcot, U.K.). The measurements were made at a fixed incident grazing angle of 1.5° using a linear detector aligned in the vertical plane. The linear detector allowed a wide range of measurement of the background scattering either side of the specularly reflected peak. Whereas this background scattering has been found to be flat over the whole range of momentum transfer ($\kappa = (4\pi \sin \theta)/\lambda$) for surfactant solutions below the cmc, this is not the case for more concentrated surfactant solutions where there is significant scattering from the micelles in the bulk of the solution (see Figure 1). The reflected signal was determined by fitting a Gaussian peak shape to the specular signal and a polynomial to the background and then subtracting an appropriate proportion

* To whom correspondence should be addressed.

® Abstract published in *Advance ACS Abstracts,* December 1, 1993.

0022-3654/93/2097-13907$04.00/0

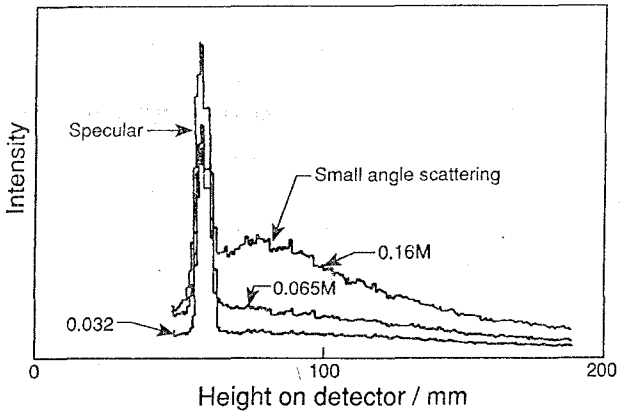

Figure 1. Specular and off-specular contributions to the reflected intensity from $hC_{14}hTAB$ in D_2O as measured on a linear multidetector oriented in the reflection plane.

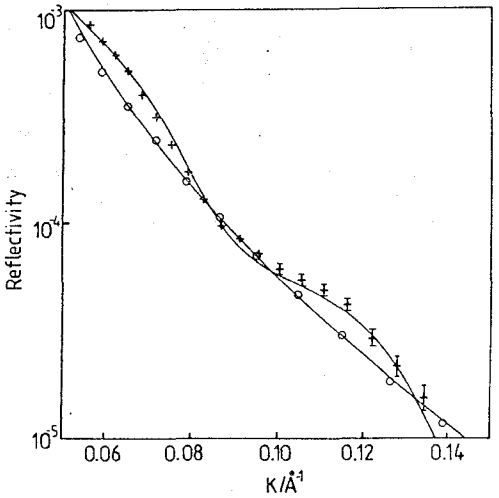

Figure 2. Neutron reflectivity profiles of fully deuterated $C_{14}TAB$ in null reflecting water at two concentrations, (O) 4.5 mM and (+) 0.16 M (T = 298 K). The background (see Figure 1) has been subtracted, and the continuous lines are (O) for a uniform monolayer (A = 44 Å^2) and (+) for the structure whose parameters are given in Table I.

of the latter to obtain the integrated specularly reflected intensity. The reflectivity curve was then calibrated with respect to that of D_2O, which had been similarly measured. The background scattering on the multidetector is higher than on a single detector because of poorer collimation, and hence the final reflectivity curves do not extend to as high a value of momentum transfer as those previously published for $C_{14}TAB$ below the cmc.

Surface tension measurements were made on a Kruss K10 tensiometer using a platinum–iridium ring. The surface tension is determined from the maximum force exerted on the ring without detachment of the meniscus. After calibration on the tension of the pure water/air interface and the heptane/water interface, standard correction factors were used to obtain the final values of the surface tension.

Results

The neutron reflectivity of $dC_{14}dTAB$ in null reflecting water (nrw) is shown as a function of concentration in Figure 2. The lowest concentration shown is just above the cmc (3.7 mM) at 4.5 mM, and the highest concentration is 0.16 M, which corresponds to about 5 wt % of the surfactant. There is a significant increase in the reflected intensity with concentration, which shows that the surface excess also increases with concentration. The fit of a single uniform monolayer structure to this data, which has been shown to be an accurate way of determining the surface excess,[3] gives the surface excesses at concentrations

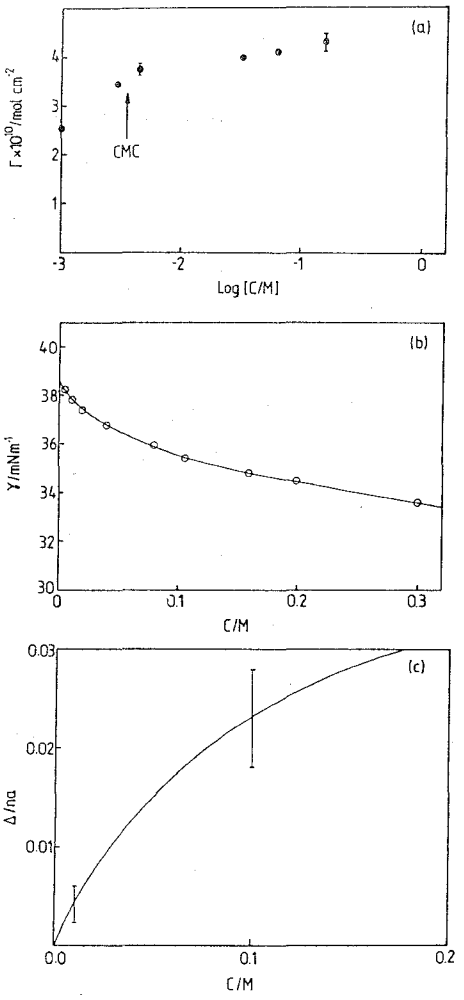

Figure 3. (a) Surface excess determined from neutron reflectivity against log(concentration). (b) Surface tension again concentration above the cmc. (c) Variation of log(mean activity of $C_{14}TAB$) with concentration, calculated from (a) and (b) using the Gibbs equation.

above the cmc. The surface excesses from the data in Figure 2 are combined with earlier measurements below the cmc in Figure 3a.[3] This figure shows that the surface excess does not reach a plateau at the cmc and hence demonstrates the dangers of using a straight line to fit the Gibbs equation in the region just below the cmc.

The values of surface excess determined by neutron reflection may be used in conjunction with surface tension measurements to determine the variation of the mean activity of the surfactant above the cmc, using the Gibbs equation in the form

$$\ln a - \ln a_{cmc} = \frac{1}{2RT}\int_{\gamma}^{\gamma_{cmc}} \frac{d\gamma}{\Gamma} = \frac{1}{2RT}\int_{\gamma}^{\gamma_{cmc}} A\, d\gamma \qquad (1)$$

where a is the mean activity coefficient, Γ is the surface excess, and A is the area per molecule. The variation of surface tension with concentration above the cmc is shown in Figure 3b and is similar to the corresponding variation for sodium dodecyl sulfate (SDS) observed by Elworthy and Mysels.[1] Within the error of the surface coverage measurements we found that A was a linear function of γ above the cmc with parameters

$$A = 1.67\gamma - 20.1 \qquad (2)$$

which gave, on substitution into eq 1 followed by integration,

$$\ln a_{cmc} - \ln a = \frac{1}{2RT}(451 + 20.2\gamma - 0.88\gamma^2) \qquad (3)$$

The change in ln a above the cmc is shown in Figure 3c with the estimated errors and is similar in general appearance to the

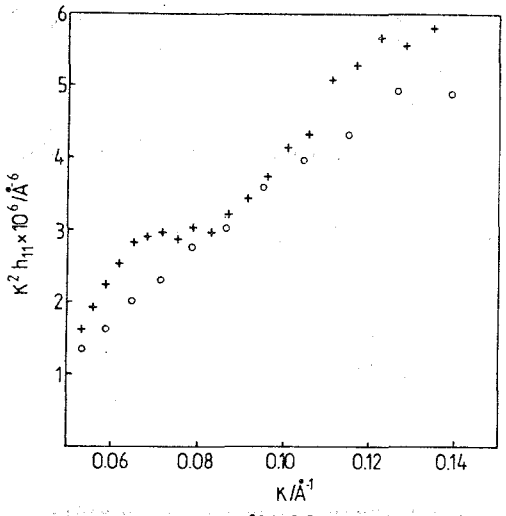

Figure 4. Partial structure factor $\kappa^2 h'$ of $C_{14}TAB$ (see eq 3) at (O) 4.5 mM and (+) 0.16 M.

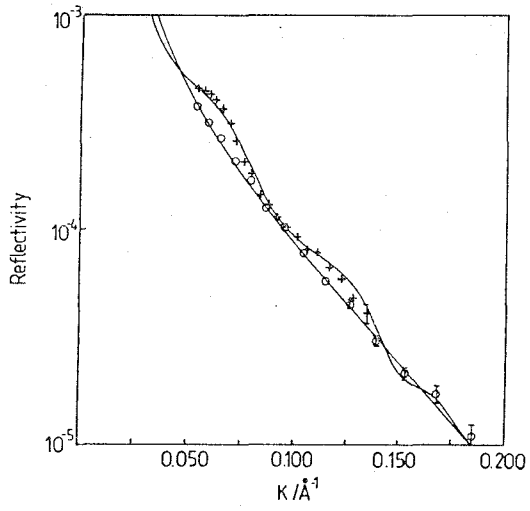

Figure 5. Neutron reflectivity profiles of fully protonated $C_{14}hAB$ in D_2O at (O) 4.5 mM and (+) 0.16 M ($T = 298$ K). The background (see Figure 1) has been subtracted, and the continuous lines are calculated for the parameters given in Table I.

corresponding variation found directly for SDS by Culter et al.,[2] although the magnitude of the change is significantly less. The value of the cmc is sufficiently low that it is a reasonable approximation to take the activity coefficient of the monomers to be unity. The value of $\Delta \ln a$ may then be used to estimate $c_\pm$ ($=(c_+c_-)^{1/2}$) for the surfactant monomer, and this is found to be very close to the value at the cmc. For example, it only rises from 3.7×10^{-3} M at the cmc to 3.8×10^{-3} M at 0.2 M. However, it should be emphasized that the concentrations of the surfactant and counterion are not necessarily the same above the cmc and may not contribute symmetrically to $c_\pm$ (see ref 2).

The most noteworthy features in the reflectivity profiles of Figure 2 are the emergence of interference features in the reflectivity profile at the highest concentration. This is shown even more clearly when the $1/\kappa^4$ decay in the reflectivity is removed as in Figure 4. The position of these features is at a κ value which suggests that they originate in surface structure with a length scale much larger than could be associated with a simple monolayer. Thus, for a monolayer of thickness 20 Å, the first noticeable feature for this contrast is a minimum at about 0.3 Å^{-1}, far beyond the features in Figures 2 and 4.

Reflectivity profiles for $hC_{14}hTAB$ in D_2O at the corresponding concentrations are shown in Figure 5. Below the cmc the reflectivity is lower than for pure D_2O, but as the concentration of surfactant increases, the reflectivity also starts to rise above that of D_2O and, just as for the measurements in nrw, interference features appear at the highest concentration.

The only possible explanation for the presence of interference effects at the low momentum transfers observed in the high-concentration reflectivity profiles of Figures 2 and 5 is that there is some kind of structure at the interface with a length scale much larger than that of a single monolayer. Since the bulk solution is a dilute solution of micelles, the most likely possibility is the formation of a layer or layers of micelles or larger aggregates at some distance from the monolayer. Larger aggregates could result if the formation of a nearby phase, near in either temperature or concentration, were induced by the planar surface (see, for example, Als-Nielsen et al.[10] and Zhou et al.[11]). The least ambiguous procedure for identifying such superstructure is to assume that there is a single layer of arbitrary thickness and composition centered at an arbitrary distance from the monolayer and then to fit the reflectivities at the two isotopic compositions to obtain the parameters of the structure. We have done this using a three uniform layer model, the first (upper) layer closely resembling the monolayer below the cmc, the second layer consisting of water and ions, and the third layer containing surfactant and water. (This is already a crude model in that earlier work has shown that the monolayer itself is best divided into two. For the D_2O profiles we included this further subdivision of the layer.) However, we found we could obtain significantly better fits to the observations if we included two further layers, although the dominant contribution to the profiles is from the top three. The parameters of the layers that best fit both isotopic data are given in Table I, and the fits themselves are shown in Figures 2 and 5. The parameters obtained are coupled to a certain extent, but two clear conclusions can nevertheless be drawn. At the highest concentration there is a surfactant layer at some distance below the surface with a concentration of surfactant of approximately 12%, and at this concentration the second (aqueous) layer contains little or no surfactant. This follows almost directly from the reflectivity in D_2O because if the scattering length density of this layer drops below that of D_2O so does the reflectivity. Indeed, there is a suggestion in the high level of the reflectivity that this aqueous layer has a net scattering length higher than D_2O. This can be seen by reference to the scattering length densities of the aqueous layers for the D_2O solutions (third layer) in Table I. For concentrations of 0.032 and 0.064 M, where only one surfactant sublayer has been included in the fitting, the scattering length density of layer three is greater than that of pure D_2O. On the other hand, for the 0.16 M, the inclusion of a second sublayer makes it possible to use a value almost identical to that of D_2O. The fact that these scattering length densities are always high is strong evidence that the surfactant concentration in this intervening aqueous layer is low because even a small amount of surfactant would cause the scattering length density to drop significantly. However, the question of whether the layer is different from bulk water remains ambiguous, and we return to this question below.

Even when surfactant is excluded from the aqueous region, the excess in the sublayer is sufficiently large to cause there to be a net excess of surfactant in the surface region over and above the surfactant in the monolayer, i.e. whatever the exact structure of layers two and three, there is overall positive adsorption of surfactant in these two layers. When the surface excess is calculated taking the positive adsorption of surfactant in the sublayers and the negative adsorption of surfactant in the first aqueous layer into account, the total excess agrees well with the corresponding value obtained by fitting a single uniform monolayer in Figure 3a. The reason for the good agreement between what are quite different structural models is partly that the overall level of the reflectivity is determined primarily by the surface excess and partly because about 95% of the excess is in the monolayer.

TABLE I: Structural Parameters Fitted Using Uniform Layer Model for 0.16 M Surfactant Solution

	1st layer		2nd layer		3rd layer		4th layer		5th layer	
conc (M)	ρ_1 (10^{-6} Å^{-2})	τ_1 (Å)	ρ_2 (10^{-6} Å^{-2})	τ_2 (Å)	ρ_3 (10^{-6} Å^{-2})	τ_3 (Å)	ρ_4 (10^{-6} Å^{-2})	τ_4 (Å)	ρ_5 (10^{-6} Å^{-2})	τ_5 (Å)
					(a) $dC_{14}dTAB$ in nrw					
0.0045	4.45	19.5								
0.032	4.67	19.5								
0.064	4.78	19.5								
0.16	4.80	19.5	0.05	33	0.80	65	0.03	30	0.5	65
					(b) $hC_{14}hTAB$ in D_2O					
0.0045	−0.25	10	2.82	10						
0.032	−0.25	10	2.82	10	6.50	15	6.2	60		
0.064	−0.25	10	2.82	10	6.50	18	6.12	60		
0.16	−0.25	10	2.82	10	6.32	33	5.70	70	6.20	28

We have previously analyzed the reflectivity of surfactant layers using partial structure factors to distinguish the contributions of the different fragments of the surfactant molecule to the structure of the layer. However, it is also possible to use the method to examine which are the most significant structural elements contributing to a given reflectivity profile, and we now use the procedure to draw less model-dependent conclusions about the structure of the interface below the monolayer. A full description of the kinematic theory is given in ref 12.

We take the structural elements to be a monolayer, m, and another surfactant layer, 1, the centers of whose distributions are δ_{m1} apart. The continuous medium is predominantly water, but we will denote it by s to show that it is not exclusively water. The reflectivity is given by

$$R = \frac{16\pi^2}{\kappa^2}(b_a{}^2 h_{mm} + b_a{}^2 h_{11} + b_s{}^2 h_{ss} + 2b_a{}^2 h_{1m} + 2b_a b_s h_{ms} + 2b_1 b_s h_{1s}) \quad (4)$$

where h_{ii} and h_{ij} are the partial structure factors, as defined in refs 5 and 13. In nrw b_w is zero, but we make the further approximation that b_s is also zero and then

$$R = (16\pi^2/\kappa^2) b_a{}^2 h' \quad (5)$$

where

$$h' = h_{mm} + h_{11} + 2h_{1m} \quad (6)$$

For the purposes of estimating the magnitude of the three contributions to h', it is convenient to take the monolayer and submonolayer surfactant distributions to be Gaussians, defined by

$$n_{ii}(z) = n_{i0} \exp(-4z^2/\sigma_i^2) \quad (7)$$

where σ_i is the full width of the distribution at 1/e of the maximum. The corresponding structure factor is

$$h_{ii}(\kappa) = (\pi \sigma_i{}^2 n_i{}^2/4) \exp(-\kappa^2 \sigma_i{}^2/8) \quad (8)$$

Since Gaussian distributions are even functions, the cross term in the partial structure factor, h_{1m}, is[5]

$$h_{1m}(\kappa) = (h_{11} h_{mm})^{1/2} \cos(\kappa \delta_{1m}) \quad (9)$$

The relative contribution of the three terms on the right-hand side of eq 4 then depends on $\sigma_1 n_{10}$ and $\sigma_m n_{m0}$. From the intensity of the subsidiary interference peaks in Figure 2 and the approximately known amount of surfactant in the monolayer, the ratio of the contributions from the two partial structure factors h_{mm}:h_{11}:$2h_{1m}$ is about 10:1:7; i.e., the two dominant contributions are from h_{mm} and h_{m1}. The contribution of h_{mm} to eq 6 may be largely eliminated by subtracting the reflectivity just above the cmc. At this concentration there is apparently no contribution from a micellar layer and the monolayer should be close to saturation. Thus, for this concentration

$$R_{cmc} \simeq (16\pi^2/\kappa^2) b_a{}^2 h_{mm} \quad (10)$$

With the assumption that h_{11} is negligible, subtraction of (10) from (5) followed by multiplication by $\kappa^2/(16\pi^2 b_a{}^2)$ gives $2h_{1m}$, which is shown in Figure 6a. Through eq 6 the partial structure h_{1m} contains most of the useful information about the submonolayer structure.

If the monolayer and micellar layer distributions are taken to be Gaussians, h_{1m} assumes the form[14]

$$h_{1m}(\kappa) = \frac{\pi \sigma_1 \sigma_m n_{m0} n_{i0}}{4} \exp\{-\kappa^2(\sigma_1{}^2 + \sigma_m{}^2)/8\} \cos(\kappa \delta_{1m}) \quad (11)$$

which is simply a Gaussian multiplied by a cosine function. That this explains the reflectivity difference at the two concentrations is demonstrated in Figure 6b,c where the best Gaussian and cosine functions that combine to give the h_{1m} in Figure 6a are drawn separately. What is clear is that the nodes in the cosine term are

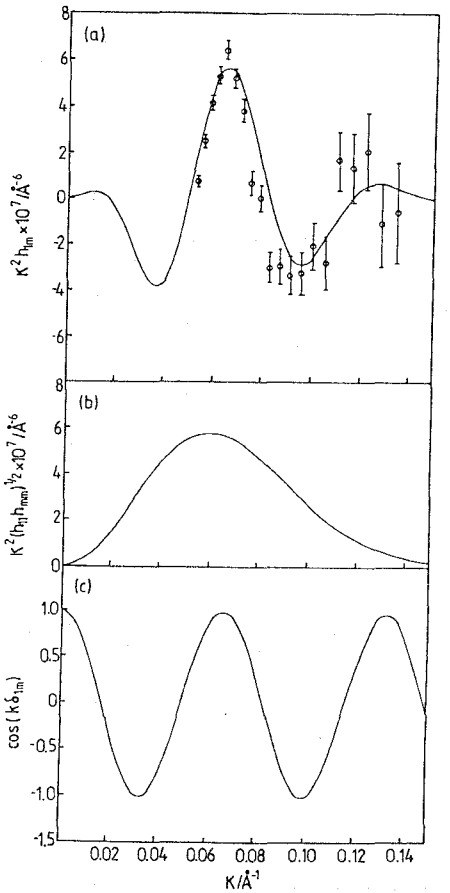

Figure 6. Approximate partial structure factor $\kappa^2 h_{1m}$ linking the subsurface surfactant and monolayer structures in the case of deuterated surfactant in nrw at 0.16 M: (a) the fit of model and experiment; (b, c) the two terms contributing to the model.

TABLE II: Structural Parameters Using the Kinematic Approximation and a Monolayer of Surfactant with a Single Submonolayer of Surfactant[a]

contrast	$10^3 n_1$/Å^{-3}	σ_1/Å	$10^4 n_m$/Å^{-3}	σ_m/Å	δ_{1m}/Å
$dC_{14}dTAB$ in nrw	1.7	17	3.3	65	95
$hC_{14}hTAB$ in D_2O	1.7	9	4	65	120

[a] The thicknesses are widths of Gaussian distributions at a height of $1/e$. In the case of $hC_{14}hTAB$ in D_2O, the thickness for the monolayer only refers to the head group region associated with water.

particularly easy to identify from the experimental results, and they give δ_{1m} directly and accurately. The Gaussian function is deduced less accurately from the overall envelope of h_{1m}. The explanation for the excess reflectivity from the submonolayer structure is accounted for exactly by this simple model. The agreement of the parameters of this result, given in Table II, with that from the model fitting is also good.

A similar analysis may be made of the reflectivities of the protonated surfactant in D_2O. All the terms in eq 4 contribute at this contrast, but b_a^2 is now very small and some of the other terms may be eliminated by subtraction of the reflectivity just above the cmc, as was done for null reflecting water. We then have

$$\Delta R = R - R_{cmc} \simeq (16\pi^2/\kappa^2)(2b_a{}^2 h_{1m} + 2b_a b_s h_{1s}) \quad (12)$$

which, since $b_a n_a$ is very much smaller than $b_s n_s$, reduces approximately to

$$\Delta R = (16\pi^2/\kappa^2) 2 b_a b_s h_{1s} \quad (13)$$

The distribution of solvent through the interface is approximately an odd one, and we may therefore write[12]

$$h_{1s} = -(h_{11} h_{ss})^{1/2} \sin(\kappa \delta_{1s}) \quad (14)$$

and, taking the simplest possible model of the solvent partial structure factor, i.e.

$$h_{ss} = n_{s0}{}^2 \exp(-\kappa^2 \tau^2) \quad (15)$$

where τ is the surface roughness, we obtain

$$h_{1s}(\kappa) = -\frac{\pi^{1/2} \sigma_1 n_{s0} n_{10}}{2} \exp\{-\kappa^2(\sigma_1{}^2 + 4\tau^2)/8\} \sin(\kappa \delta_{1s}) \quad (16)$$

Just as for the deuterated surfactant in nrw this has the form of a modulated Gaussian, but this time by $\sin(\kappa\delta_{1s})$. The observed h_{1m} is shown in Figure 7a, together with the best fit of eq 16, and the separate components of the equation are shown in Figure 7b,c. The value of δ_{1s} is once again the most accurately determined parameter of the profile. Its value of 120 Å agrees approximately with that of δ_{1m} of 95 Å (see Table II for the set of fitted parameters). There should be a small difference between the two δ values because the one measures the distance from the subsurface surfactant layer to the center of the monolayer and the other to the center of the water distribution, and the latter two distributions are separated by 5–10 Å. However, this difference is probably swamped by errors introduced by the simplified model.

In Figure 7a the experimental curve has been scaled to highlight the interference effect. However, the actual reflectivity of the 5% solution is higher than can be explained by the model of the surface structure so far given. This is shown in Figure 8a where the true solvent partial structure factor is shown to be about 20% greater than the scaled version (Figure 8b), which was used to obtain the data in Figure 7. We previously observed the same effect for $C_{10}TAB$ solution and parametrized it in terms of an anomalously high density of water in the aqueous layer just below the surfactant monolayer. The effect appears to be a genuine one, outside the normal range of scaling errors of about 10%. In the discussion above concerning the optical matrix fitting of the

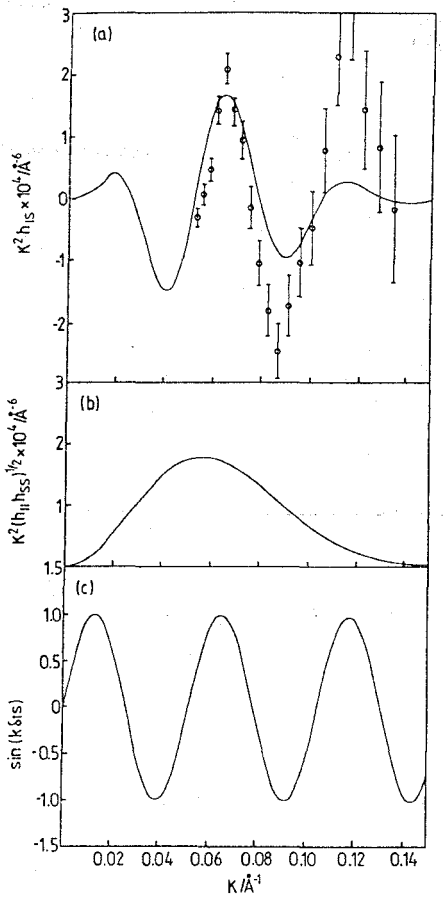

Figure 7. Approximate partial structure factor $\kappa^2 h_{1s}$ linking the subsurface surfactant and monolayer structures in the case of protonated surfactant in D_2O at 0.16 m: (a) the fit of model and experiment; (b, c) the two terms contributing to the model.

data, we indicated that there were two possible explanations of the high reflectivity, the first arising from more extensive layering of surfactant and the second from an apparent anomalously high scattering length density of water. We now consider the second possibility. The idea of a layer of water more dense than the bulk seems implausible. An alternative is that there is some structuring in the water in the direction normal to the surface, such as has been observed in mica force balance experiments.[14] The reflectivity is a nonlinear function of the scattering length density profile, and it is therefore possible for it to be anomalously high for a solvent distribution suitably structured in the direction normal to the surface. A simple analysis using the kinematic approximation shows that a form of scattering length density distribution which involves no change in the average density but which causes the reflectivity to be enhanced above that from a uniform solvent is that shown as a continuous line in Figure 9a. The corresponding partial structure factor is given by

$$\kappa^2 h = n^2\{1 + 8A(2A-1)\sin^2(\kappa d/2) + 4A(1-A)\sin \kappa d\} \quad (17)$$

where A is an extra scattering length density relative to the average density of the bulk. For dimensions of a water molecule of about 4 Å and for positive values of A, $\kappa^2 h$ approaches the limiting value of n^2 from above as κ tends to zero (continuous lines in Figure 9b), and the enhancement is about 20% at $\kappa = 0.05$ Å^{-1} when $A \simeq 1.25$. Since the reflectivity is obtained simply by multiplying by κ^4, the reflectivity will also be anomalously high at low angles. Reversal of the two layers (Figure 9a, dashed line) reverses the direction of approach to the limiting value at $\kappa = 0$. In this case

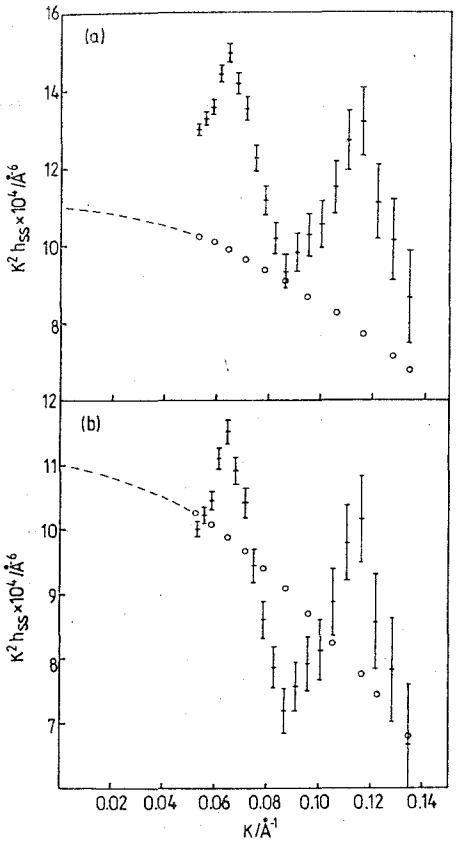

Figure 8. Solvent partial structure factor $\kappa^2 h_{ss}$ at (O) 4.5 mM and (+) 0.16 M (a) as obtained directly from the reflectivities and (b) scaled as used for Figure 7.

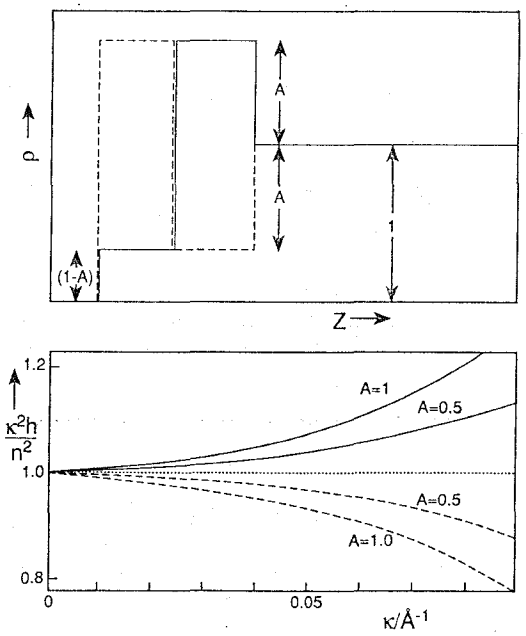

Figure 9. Effect of solvent structuring on the solvent partial structure factor. (a) Scattering length density profiles that enhance the reflectivity at low κ (continuous line) and depress it (dashed line). (b) Calculated $\kappa^2 h/n^2$ for different values of the parameter A in eq 17 (continuous lines) and in eq 18 (dashed lines). The partial structure factor for the perfectly smooth solvent is shown as a dotted line.

$$\kappa^2 h = n^2\{1 + 8A(2A + 1)\sin^2(\kappa d/2) - 4A(1 + A)\sin \kappa d\} \quad (18)$$

for which $\kappa^2 h$ is shown as dashed lines for two values of A in Figure 9b. Also included for comparison in Figure 9b is the behavior for a perfectly smooth surface (dotted line). The

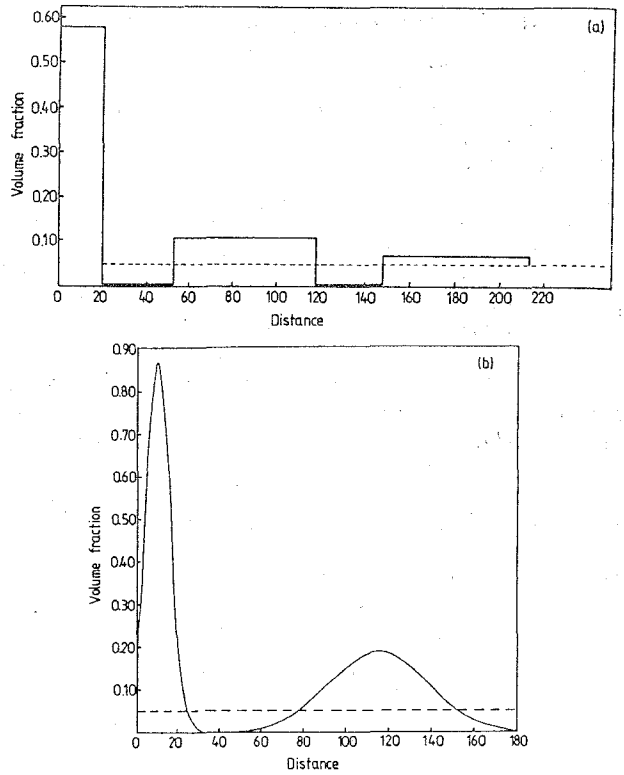

Figure 10. Volume fraction profile of C_{14}TAB normal to the interface for (a) the best uniform layer model (see Table Ia for the width parameters in each layer) and (b) from direct fitting of the partial structure factors. The number density of the micellar layer is taken to be the average of the values fitted from the two contrasts as listed in Table Ib.

inclusion of roughness, of whatever kind, would damp out these effects of structuring on the reflectivity, especially at higher κ. Nevertheless, this explanation of the anomalously high reflectivities in D_2O makes it possible that there is some contribution to the reflectivity from a structured layer of water. This does seem surprising since the roughness of the surface is expected to be greater than the dimensions of a water molecule. If the water were structured, it would have some consequences for the interpretation of the reflectivity from the surfactant, but the crude models used earlier for the analysis do not warrant the extra detail.

Discussion

The most striking observation from the present results is the formation of a micellar layer below the surface with a net adsorption of surfactant over and above the amount in the monolayer. The distribution obtained by fitting the reflectivity using a sequence of uniform layers and an exact calculation of the reflectivity is shown in Figure 10a and that for the more direct, but approximate, analysis in Figure 10b. Both distributions are plotted in the form of volume fraction profile through the interface. Although there are some differences between the two profiles, they give the same semiquantitative result in terms of dimensions and surface excess.

The amount of surfactant in the subsurface layer and its dimensions strongly suggest that this layer consists of micelles at about double the bulk concentration. The diameter of C_{14}-TAB micelles has been determined by several authors, e.g., Berr et al.[16] At a concentration corresponding to that of our experiment, the micelles are thought not to be perfectly spherical and the mean diameter is in the range 45–55 Å. This is slightly smaller than either of the distributions in Figure 9, but in the case of the micellar layer there will be an additional contribution from diffuseness of the layer. If the layer were a defective bilayer, its

thickness would be expected to be substantially less than the 65 Å observed.

The formation of the micellar layer in itself is not so surprising. Many computer simulations have predicted oscillations in the density profile near a hard wall (e.g. ref 17), and experimentally such effects have been observed for fluids in the force balance apparatus,[14] although none involving micelles which should be observable. Most striking are the computer simulations of Smit et al.,[8,9] which showed such an ordering for micelles at the oil/water interface. The air/solution interface is not a hard wall in that it is roughened by thermal motions. However, the root-mean-square amplitude of these fluctuations will be of the order of 5 Å, which is small in comparison with the diameter of the micelles ($\simeq$50 Å).

Although the depletion of micelles from a region with a thickness of the order of the diameter of the micelles is not surprising, the excess concentration of the micelles in the layer below the depletion layer is less easily explained. This excess is sufficiently large to give a net surface excess of micelles. This excess concentration can result only if the interaction (integrated over the whole distance of the interaction) of a micelle with the monolayer is more attractive, or less repulsive, than the interaction of the micelle with bulk micellar solution. Unfortunately, the dimensions of the micelles are too small for it to be possible to scale the interaction for different shaped particles using the Derjaguin recipe,[18] and there is considerable uncertainty in the quantitative detail of the double-layer interaction itself. However, the separation of micelles from the monolayer, at about 100 Å, is less than the mean separation of 150 Å in the bulk solution (at 0.16 M). This is consistent with either the repulsion between monolayer and micelle being less than that between micelle and bulk micellar solution or the attraction between monolayer and micelle being greater than that between micelle and bulk.

Acknowledgment. E.A.S. thanks the Science and Engineering Council and Unilever Research, Port Sunlight, for support.

References and Notes

(1) Elworthy, P. H.; Mysels, K. J. *J. Colloid Interface Sci.* **1966**, *21*, 331.
(2) Cutler, S. G.; Meares, P.; Hall, D. G. *J. Chem. Soc., Faraday Trans. 1* **1978**, *74*, 1758.
(3) Simister, E. A.; Thomas, R. K.; Penfold, J.; Aveyard, R.; Binks, B. P.; Cooper, P.; Fletcher, P. D. I.; Lu, J. R.; Sokolowski, A. *J. Phys. Chem.* **1992**, *96*, 1383.
(4) Tajima, K.; Muramatsu, M.; Sasaki, T. *Bull. Chem. Soc. Jpn.* **1970**, *43*, 1991.
(5) Simister, E. A.; Lee, E. M.; Thomas, R. K.; Penfold, J. *J. Phys. Chem.* **1992**, *96*, 1373.
(6) Lee, E. M.; Simister, E. A.; Thomas, R. K.; Penfield, J. *J. Phys. (Paris)* **1989**, *50-C-7*, 75.
(7) Lee, E. M.; Thomas, R. K.; Penfold, J.; Ward, R. C. *J. Phys. Chem.* **1989**, *93*, 381.
(8) Smit, B.; Hilbers, P. A. J.; Esselink, K.; Rupert, L. A. M.; van Os, N. M.; Schlijper, A. G. *Nature* **1990**, *348*, 624.
(9) Smith, B.; Hilbers, P. A. J.; Esselink, K.; Rupert, L. A. M.; van Os, N. M.; Schlijper, A. G. *J. Phys. Chem.* **1991**, *95*, 6361.
(10) Pershan, P. S.; Braslau, A.; Weiss, A. H.; Als-Nielsen, J. *Phys. Rev. A* **1987**, *35*, 4800.
(11) Zhou, X. L.; Lee, L. T.; Chen, S. H.; Strey, R. *Phys. Rev. A* **1992**, *46*, 6479.
(12) Lu, J. R.; Simister, E. A.; Lee, E. M.; Thomas, R. K.; Rennie, A. R.; Penfold, J. *Langmuir* **1992**, *8*, 1837.
(13) Lu, J. R.; Li, Z. X.; Su, T. J.; Thomas, R. K.; Penfold, J. *Langmuir* **1993**, *9*, 2408.
(14) Israelichvili, J. N. *Intermolecular and Surface Forces*, 2nd ed.; Academic Press: London, 1992.
(15) Lu, J. R.; Hromadova, M.; Thomas, R. K.; Penfold, J. *Langmuir* **1993**, *9*, 2417.
(16) Berr, S. S.; Jones, R. R. M.; Johnson, J. S. *J. Phys. Chem.* **1992**, *96*, 5611.
(17) Nicholson, D.; Parsonage, N. G. *Computer Simulation and the Statistical Mechanics of Adsorption*; Academic Press: London, 1982.
(18) Hunter, R. J. *Foundations of Colloid Science*; Clarendon Press: Oxford, 1989; Vol. I.